Structure of birnavirus-like particles determined by combined electron cryomicroscopy and X-ray crystallography

Joan Pous, Christophe Chevalier, Malika Ouldali, Jorge Navaza, Bernard Delmas, Jean Lepault

Journal of General Virology (2005), **86**, 2339–2346 DOI 10.1099/vir.0.80942-0

Structure of birnavirus-like particles determined by combined electron cryomicroscopy and X-ray crystallography

Joan Pous,[1] Christophe Chevalier,[2] Malika Ouldali,[1] Jorge Navaza,[1] Bernard Delmas[2] and Jean Lepault[1]

[1]Laboratoire de Virologie Moléculaire et Structurale, UMR 2472 CNRS-INRA, 1 avenue de la terrasse, F-91198 Gif-sur-Yvette, France

[2]Unité de Virologie et Immunologie Moléculaires, Domaine de Vilvert, INRA, F-78350 Jouy-en-Josas, France

Correspondence
Bernard Delmas
delmas@jouy.inra.fr

Jean Lepault
lepault@vms.cnrs-gif.fr

Received 2 February 2005
Accepted 21 April 2005

Birnaviruses possess a capsid with a single protein layer in contrast to most double-stranded RNA viruses infecting multicellular eukaryotes. Using freeze-drying and heavy metal shadowing, the capsids of two birnaviruses, infectious bursal disease virus (IBDV) and infectious pancreatic necrosis virus, as well as of an IBDV virus-like particle (VLP) are shown to follow the same T = 13 laevo icosahedral geometry. The structure of the VLP was determined at a resolution of approximately 15 Å (1·5 nm) by a combination of electron cryomicroscopy and a recently developed three-dimensional reconstruction method, where the scattering density is expressed in terms of symmetry-adapted functions. This reconstruction methodology is well adapted to the icosahedral symmetry of viruses and only requires a small number of images to analyse. The atomic model of the external capsid protein, VP2, recently determined by X-ray crystallography, fits well into the VLP reconstruction and occupies all the electron densities present in the map. Thus, similarly to the IBDV virion, only VP2 forms the icosahedral layer of the VLP. The other components of both VLP and IBDV particles that play a crucial role in the capsid assembly, VP1, VP3 and the peptides arising from the processing of pVP2, do not follow the icosahedral symmetry, allowing them to be involved in other processes such as RNA packaging.

INTRODUCTION

Double-stranded RNA (dsRNA) virus particles are complex transcription machineries. The genome of these viruses has to be hidden from the cellular defence mechanisms at all steps of the viral life cycle. Viral dsRNA is thus confined in the capsid and transcribed mRNAs are extruded through pores located at the virion fivefold axes (Prasad *et al.*, 1996). The capsid of dsRNA viruses is generally formed by a layer of protein that displays an icosahedral symmetry, T = 1, with two subunits in the asymmetric unit (Caston *et al.*, 1997; Grimes *et al.*, 1998; Reinisch *et al.*, 2000). Although cypoviruses are single shelled (Hill *et al.*, 1999), the capsid of most dsRNA viruses that replicate in multicellular eukaryotes such as viruses of the family *Reoviridae*, displays additional protein layers that give to the particles a multilayer appearance when observed by electron microscopy. Some and often all additional layers possess a T = 13 icosahedral symmetry (Grimes *et al.*, 1998; Reinisch *et al.*, 2000; Roseto *et al.*, 1979), an intriguing characteristic feature of dsRNA viruses.

Birnaviridae is a dsRNA virus family with members infecting numerous animal species. They have two genomic segments (Dobos *et al.*, 1979) contained within a capsid formed by a single protein layer with T = 13 icosahedral symmetry (Bottcher *et al.*, 1997). The chirality of the lattice was reported to be laevo or dextro depending upon the birnavirus species (Ozel & Gelderblom, 1985). The most studied birnaviruses are the infectious bursal disease virus (IBDV) and infectious pancreatic necrosis virus (IPNV) (Muller *et al.*, 2003; Rodriguez Saint-Jean *et al.*, 2003). IBDV and IPNV cause important economical losses to poultry and fish industries, respectively.

The capsid morphogenesis of birnaviruses requires the presence of four proteins: VP1, pVP2, VP3 and VP4 (Chevalier *et al.*, 2004). VP1 is the RNA-dependent RNA polymerase and is coded by genomic segment B (von Einem *et al.*, 2004). VP4 is the viral protease and arises from the autocatalytic cleavage of the polyprotein NH_2-pVP2-VP4-VP3-COOH that is coded by genomic segment A (Birghan *et al.*, 2000). While minor amounts of VP1 and negligible quantities of VP4 are incorporated both in virus and virus-like particle (VLP), VP2 and VP3 are the major components of the particles (Lombardo *et al.*, 1999; Muller & Becht, 1982). The latter are present in roughly equimolar amount in IBDV

particles (Chevalier *et al.*, 2002, 2004). During capsid assembly, the C terminus of pVP2 is processed by VP4, giving rise to VP2, the external capsid protein and four peptides that all stay closely associated with the capsid (Da Costa *et al.*, 2002). Because VP3 is present in large quantities within the capsid, it was considered as a component of the icosahedral shell of the virus (Bottcher *et al.*, 1997). Interestingly, it was found that the presence of VP1 is not a prerequisite for VLP assembly (Fernandez-Arias *et al.*, 1998). However, in the baculovirus/Sf9 cell expression system and in the absence of VP1, we observed that the formation of VLP requires the C terminus of VP3 to be deleted or fused with an exogenous protein such as the green fluorescent protein (GFP) (Chevalier *et al.*, 2002, 2004). Indeed, VLP assembly requires the charged C-terminal domain of VP3 to be removed or to be shielded by endogenous (VP1) or exogenous proteins (GFP). Moreover, VP3 has recently been shown to interact with the C-terminal domain of pVP2 (Ona *et al.*, 2004).

To clarify the central role of VP3 in birnavirus assembly, we determined the three-dimensional structure of the IBDV-VLP by electron cryomicroscopy and image processing techniques. The presence of the GFP-fused VP3 inside the capsid might change the mobility and/or flexibility of VP3 and thus facilitate its localization in the VLP three-dimensional map. Although a dextro lattice has been previously proposed (Ozel & Gelderblom, 1985), the fitting of the VP2 atomic model in the electron cryomicroscopy map (Bottcher *et al.*, 1997) suggested an opposite hand (Coulibaly *et al.*, 2005). Thus, we first determined the hand of the VLP and both IBDV and IPNV using the heavy metal shadowing technique. Shadowing only visualizes one surface and thus allows hand determination. To maximize the structural preservation of the object during drying, we used freeze-drying (Roseto *et al.*, 1979) with bacteriophage T4 tail as an internal reference (Bayer & Remsen, 1970). VLP, IBDV and IPNV all display a T = 13 laevo icosahedral geometry. Second, using electron cryomicrographs of VLP, we determined the structure of the VLP at a resolution of approximately 15 Å (1·5 nm) using a three-dimensional reconstruction method, where the angular part of the scattering density is expressed as symmetry adapted linear combination of spherical harmonics (Navaza, 2003). We show that, in spite of the presence of GFP fused to its C terminus, VP3 is not visible in the VLP. The ordered density in the reconstruction corresponds exclusively to VP2, demonstrating that the affinity between VP2 and VP3 is weak and that the icosahedral capsid contains VP3 molecules that do not follow icosahedral symmetry. The atomic model of the capsid protein, VP2 fits well into the VLP reconstruction. The VLP quasi-atomic model is similar to the crystallographic model of the IBDV particle recently determined, demonstrating that the capsid structure does not greatly depend on the presence of the genomic RNA. VP3 thus appears to have a dual function: although it does not follow the icosahedral symmetry, VP3 controls assembly of the T = 13 laevo capsid and, due to its RNA affinity, might be involved in other processes such as genomic RNA packaging.

METHODS

Viruses. The Gumboral CT IBDV vaccine strain was kindly provided by Mérial. IPNV was prepared as described by Galloux *et al.* (2004). Briefly, the virus was grown in a rainbow trout gonad-2 cell line and precipitated from the culture medium by adding polyethylene glycol 6000 (PEG 6000) at a 10 % (w/v) final concentration. Overnight PEG 6000 precipitation was followed by a low speed centrifugation. The pellet was resuspended in 50 mM Tris/HCl, pH 7·4, 150 mM NaCl. This procedure permits virus concentration avoiding ultracentrifugation steps that damage the virions. Finally, just before use, the viruses were purified by size exclusion chromatography on a Sepharose 200 column (Pharmacia).

Recombinant VLP production. The baculovirus expressing the IBDA polyprotein fused at its C terminus with the GFP protein has been described previously (Chevalier *et al.*, 2002). Sf9 cells were infected at an m.o.i. higher than 5 p.f.u. ml^{-1} in the presence of protease inhibitors leupeptin (0·5 μg ml^{-1}) and aprotinin (1 μg ml^{-1}). Cell cultures were collected 100 h post-infection after addition of the same protease inhibitors at the same concentrations and treated with Vertrel XF (Dupont de Nemours). Purification was carried out by caesium chloride density-gradient centrifugation as described previously (Chevalier *et al.*, 2002). The protein concentrations were estimated by the method of Bradford (1976) using bovine serum albumin as a standard and/or UV spectrophotometry at 280 nm.

Electron microscopy. Specimens were prepared from the appropriate caesium chloride gradient fraction, containing the different assembled forms, by desalting through Micro Bio-Spin chromatography columns (Bio-Rad) equilibrated with a buffer containing 50 mM Tris/HCl pH 7·4, 150 mM NaCl. All the samples were first analysed by negative staining (not shown).

Freeze-drying and shadowing were done as described previously (Lepault *et al.*, 1981). Samples were adsorbed onto air glow-discharged carbon coated grids. The excess solvent was removed and the grids frozen by plunging into liquid nitrogen. The grids were transferred into a Reichert device (Escaig & Nicolas, 1976) and maintained at −80 °C for 2 h. They were then shadowed with a 20 Å (2 nm) thick layer of carbon-platinum evaporated under an elevation angle of 30 degrees. The replicas were coated with a 200 Å (20 nm) thick carbon layer. Grids were observed in a CM12 electron microscope (Philips) operated at 80 kV.

Electron cryomicroscopy was performed as described previously (Dubochet *et al.*, 1988) by using a Philips CM12 electron microscope and a Gatan 623 cryoholder. Micrographs defocused by 1·5–2·5 μm were recorded at a nominal magnification of 35000 on Kodak SO163 Electron Plate, developed 12 min in Kodak D19. The scanned micrographs were visualized with Photoshop (Adobe Systems).

Three-dimensional reconstructions. Micrographs were scanned with a Nikon Coolscan 8000 at a resolution of 4000 d.p.i. that corresponds to a pixel size of 1·8 Å (0·18 nm). A total of 189 individual particles were selected from three micrographs using the program x3d (Conway & Steven, 1999). Every centre of mass was then calculated after reducing the resolution to 15 Å (1·5 nm) and smoothing the resulting map by using a 5 Å (0·5 nm) Wang filter (Wang, 1985).

The three-dimensional reconstruction was made using the RICO suite of programs (Navaza, 2003). The protocol consists of three main steps: (i) preparation of data, (ii) search of the views of the

individual projections and (iii) building the final reconstruction. First, the images were Fourier-Bessel transformed and sampled on 500 equidistant reciprocal pixels in the 0·0 to 0·1 $Å^{-1}$ (0·0 to 0·01 nm^{-1}) range. Only angular frequencies (pulsations) below 200 where retained. Second, for each image and all possible view angles in 3 degrees steps, low-resolution icosahedral reconstructions were calculated by using the first 150 sampling points [0·03 $Å^{-1}$ (0·003 nm^{-1})] and including angular frequencies only up to 30. Each of these reconstructions was then projected and correlated to the original image. The view parameters of the best-correlated reconstruction were taken as a reference and the view parameters of the rest of the images were redetermined and refined taking the reference into account. The centre of each projection was also refined. An important feature of the reconstruction method was that no model is necessary (Navaza, 2003). Another cycle of view/centre refinement was carried out at higher resolution using angular frequencies up to 50 and 250 reciprocal pixels [0·05 $Å^{-1}$ (0·005 nm^{-1})].

The third step consisted in building the final reconstruction from the oriented and centred images. For this, the complete Fourier-Bessel expansion was used up to a resolution of 15 Å (1·5 nm). This procedure gave a map for each of the three micrographs. These were independently corrected for CTF effects. The zeros of the transfer function were searched as described previously (Conway & Steven, 1999). Phase-flip corrections were calculated for each group of images (Erickson & Klug, 1971). To minimize the introduction of noise in the reconstructions, data near the zeros of the CTF functions were eliminated. These three CTF corrected Fourier transforms were combined and softened by using a 5 Å (0·5 nm) Wang filter (Wang, 1985). Some disconnected density blobs were eliminated using the program Unblob (Conway & Steven, 1999).

Fitting of the atomic model into the VLP reconstruction. The complete virus capsid of IBDV or the 13 VP2 monomers contained in the asymmetric unit were fitted in to the VLP reconstruction by using the program URO (Navaza *et al.*, 2002). The resolution of the experimental map was estimated by comparison with the resulting calculated model limited at different resolutions. All the figures of maps and protein coordinates were rendered by using the program PyMOL (W.L. DeLano, 'The PyMOL Molecular Graphics System'; DeLano Scientific LLC. http://www.pymol.org).

RESULTS

Protein composition of IBDV virion and VLP

IBDV particles mainly contain five proteins: VP1, pVP2, VP2, VP3 and VP4 (Fig. 1). While VP2 and VP3 are the major proteins of the viral particles, their relative amounts vary from one preparation to another. In general, VP3 is present in larger quantities than VP2 in the virus as detected by SDS-PAGE and Coomassie blue staining. In our IBDV samples, pVP2 species and VP4 are very minor components. When the IBDV polyprotein (segment A) is expressed in the insect cell baculovirus-expressing system, in the absence of VP1 (segment B), the efficient formation of VLP requires an exogenous polypeptide, such as the GFP, to be fused at the C terminus of VP3 (Chevalier *et al.*, 2002, 2004). Three proteins mainly constitute the VLP: VP3–GFP, pVP2 and VP2. Different maturation forms of pVP2 are observed (Fig. 1). VP4 is generally not detected in purified VLP samples. In addition, four peptides arising from the maturation of pVP2 are detected by mass spectrometry in the VLP and virion (Da Costa *et al.*, 2002).

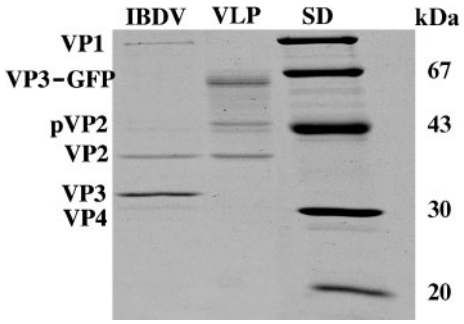

Fig. 1. Identification of the polypeptides constituting IBDV virions (IBDV) and virus-like particle (VLP) by SDS-PAGE analysis and Coomassie blue staining. Protein assignment was carried out by trypsin digestion and MALDI-TOF analysis. Note that in all cases VP3 appears to be more abundant than VP2. The relative molecular mass of standard proteins (SD) is indicated on the right.

Hand of IBDV virion and VLP

Fig. 2 shows IBDV, IPNV and recombinant IBDV-VLP freeze-dried and then shadowed with a thin carbon-platinum film. To avoid any error in the hand determination that may arise from an inversion of the grid in the microscope or an inversion of the negative, we used the tail of the bacteriophage T4 as a reference. The long pitch helices constituting the external surface of the extended conformation of the T4 tail are right handed, they slope upwards from left to right (Bayer & Remsen, 1970). On the left part of Fig. 2, low magnification pictures show viruses and VLP together with T4 bacteriophage. The surface lattice gives the particles, virion and VLP the appearance of a golf-ball. This impression is even more obvious at higher magnification when a local Gaussian averaging is applied (Fig. 2, right panels). Two different depressions on the surface, presenting five- and sixfold local symmetry are visible on the particle surface. To simplify the description, depressions will be referred to as holes from here onwards. To determine the triangulation number and the hand of the lattice, the shortest walk joining two fivefold holes through sixfold holes has to be defined. For all the particles observed, IBDV, IPNV and IBDV-VLP, the shortest path from a fivefold hole to its closest fivefold neighbour is a walk through three aligned sixfold holes and a left (laevo) turn towards the contiguous fivefold hole. Such a geometry demonstrates that IBDV virions (Fig. 2, upper row), IPNV virions (Fig. 2, middle row) and recombinant IBDV-VLP (Fig. 2, lower row) all display a $T=13$ laevo icosahedral symmetry.

Five- and sixfold holes have characteristic structures. Although fivefold holes are smaller than sixfold ones, pentamers have stronger contrast than hexamers. In the printing convention used in Fig. 2, VP2 pentamers appear whiter than hexamers and are thus easily discerned.

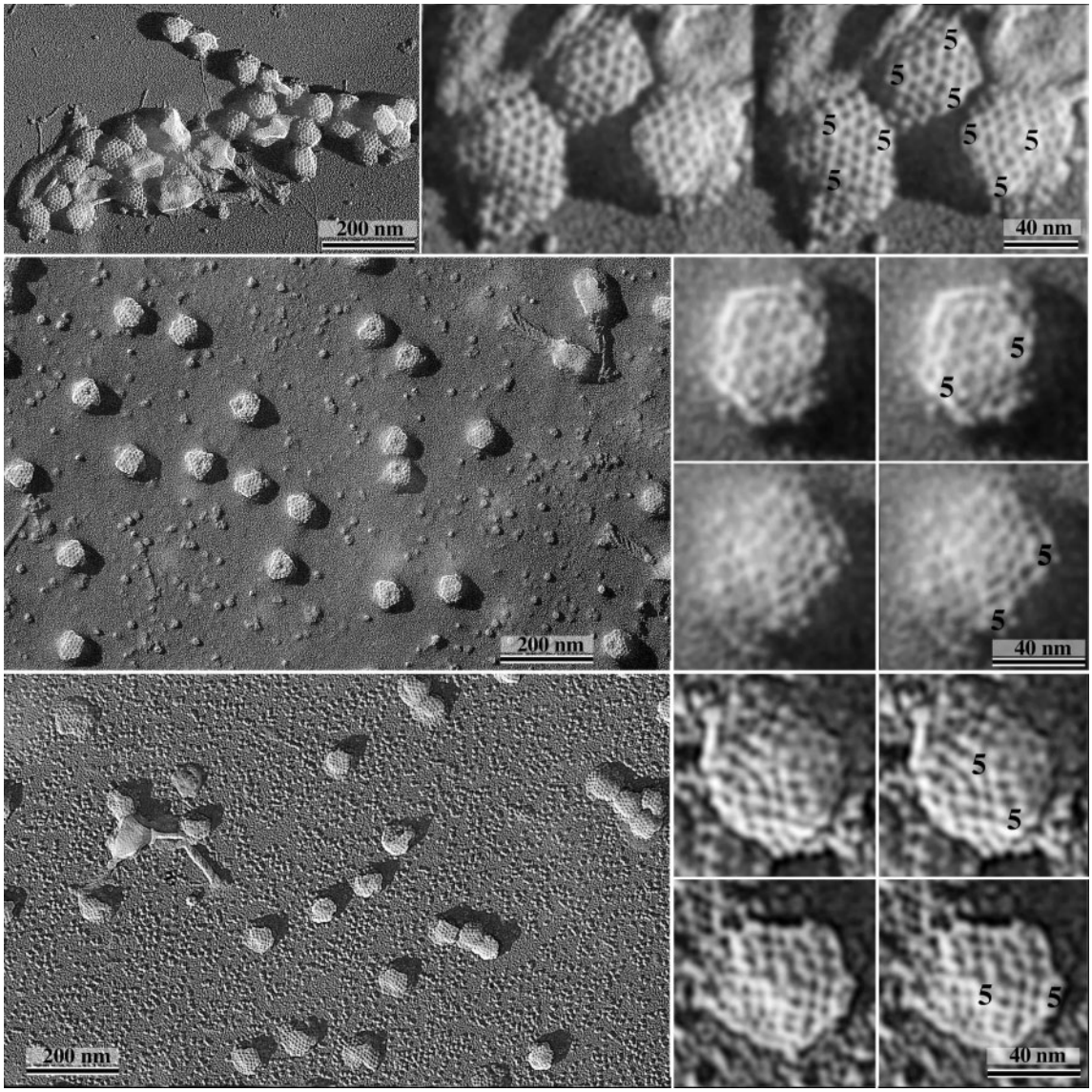

Fig. 2. Visualization of the surface structure of viruses and VLP by freeze-drying and heavy metal shadowing. In all studied cases, T4 bacteriophages were added to the samples; the right-handed long-pitch helices of the T4 tail (Bayer & Remsen, 1970) was used as a reference. All tails show oblique striations that slope upwards from left to right. IBDV virions, upper row; IPNV virions, middle row; and IBDV-VLP, lower row, were studied. The structure of the particle surface gives the appearance of a golf-ball at low magnification (left panels). Five- and sixfold holes are visible, particularly at high magnification (right panels). In all cases, the lattice defined by the five- and sixfold holes is characteristic of T = 13 laevo icosahedral particles. The right panels show two identical images; the fivefold holes are indicated on the left duplicate.

The IBDV, IPNV and IBDV-VLP samples differ by their structural preservation after freeze-drying. These differences arise from different physical properties of the particles. IPNV is more fragile than IBDV and is damaged during ultracentrifugation (Galloux *et al.*, 2004). As a consequence, in the background of IPNV samples, numerous small entities arising from partial particle degradation are visible (Fig. 2, central panel). These small objects are likely VP2 aggregates. In addition, flattening is generally observed when particles are adsorbed on a supporting film. IBDV-VLPs have an even stronger tendency than virions to flatten (Fig. 2, lower panel). This effect is attributed to the fact that VLPs are empty particles as far as RNA is concerned and therefore more deformable.

IBDV virions and VLPs have similar surface structures. VP3 has not been detected in the virus by X-ray crystallography (Coulibaly *et al.*, 2005). In the VLP, a 25 kDa protein, the GFP, is fused to the C terminus of VP3 and may prevent VP3 movement. Fused to GFP, VP3 might thus be detected in VLP three-dimensional reconstructions.

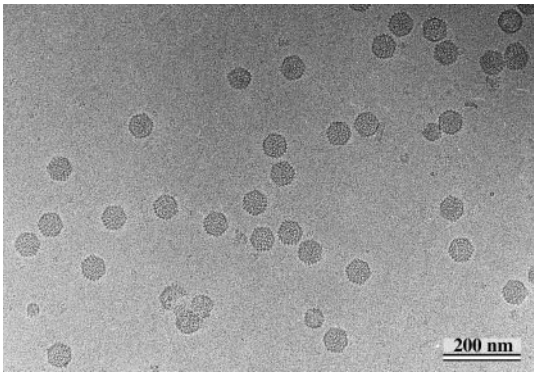

Fig. 3. Images of IBDV-VLP containing the fusion protein VP3–GFP embedded in ice. Although a few particles are damaged, most of them show the characteristic appearance of icosahedral viruses.

Three-dimensional structure of VLP

Fig. 3 shows IBDV-VLP embedded in a vitreous ice layer. While very few particles appear damaged, most of the particles display a uniform diameter and show the characteristic pattern of icosahedral objects. The three-dimensional structure was calculated with a new program based on the decomposition of the object density in a symmetry-adapted combination of spherical harmonics (Navaza, 2003). Fig. 4 shows the reconstruction calculated with 189 particles. The reconstruction confirmed that the VLP is organized with a T = 13 geometry. In view of the shadowing experiments, a laevo conformation was imposed to the lattice in the reconstruction. Two different domains can be seen in the capsid: a rather continuous layer forming a shell (Fig. 4, S) and an elongated projecting domain forming a spike (Fig. 4, P) on the surface of the shell. The spikes define five- and sixfold depressions. In agreement with the rotary shadowing observations, the fivefold holes are smaller than the sixfold ones. The VLP reconstruction is indeed highly similar to that of the virion (Bottcher *et al.*, 1997; Caston *et al.*, 2001).

The atomic model of VP2 fits well into the reconstruction (Fig. 5). The VP2 envelope defined in the microscopy map surrounds most of the VP2 residues. However, the last 15 residues of VP2 that are ordered in the virion (Coulibaly *et al.*, 2005) appeared disordered in the VLP. These residues are not included in the microscopy VP2 envelope (Fig. 5, arrow). In addition, the VP2 molecule occupies all the density that can be attributed to protein. There is no extra density that can be assigned neither to VP3–GFP nor even to the peptides arising from the processing of pVP2. Only VP2 appears to obey to icosahedral symmetry in IBDV-VLP.

DISCUSSION

All characterized dsRNA viruses of the family *Reoviridae* have a core surrounded by a capsid shell that displays a T = 13 laevo geometry, whether they infect plants or animals: rice dwarf virus (Lu *et al.*, 1998; Nakagawa *et al.*, 2003), rotavirus (Ludert *et al.*, 1986; Roseto *et al.*, 1979), blue tongue virus (Grimes *et al.*, 1998; Prasad *et al.*, 1992) and reovirus (Metcalf *et al.*, 1991; Reinisch *et al.*, 2000). Viruses of the *Birnaviridae*, a different dsRNA virus family, infect various animal species and also present a capsid having a T = 13 icosahedral geometry (Bottcher *et al.*, 1997). However, lattices of different hand, laevo and dextro, have been reported for different viruses (Ozel & Gelderblom, 1985). In particular, IBDV and IPNV, the most studied birnaviruses have been reported as having opposite hands, although their major capsid proteins present high amino acid sequence conservation (about 40 and 35 % for VP2 and VP3, respectively). The hand of a lattice is difficult to determine by electron microscopy because grids or micrographs are easily flipped upside down during the analysis. An internal reference avoids eventual errors. The hand of IBDV and IPNV icosahedral lattices were thus revisited by using the long-pitch helices of the bacteriophage T4 tail (Bayer & Remsen, 1970) as a reference. Thus, we showed that IBDV, IPNV and IBDV-VLP have the same hand: both viruses display a T = 13 laevo icosahedral symmetry. Interestingly, it appears that only dsRNA viruses have a T = 13 icosahedral capsid, and in addition they all display a laevo configuration. These common properties suggest that T = 13 laevo dsRNA viruses might arise from a common ancestor. Comparison of the atomic structure of the capsid protein forming a T = 13 layer in IBDV (VP2) and in viruses of the *Reoviridae* (rotavirus VP6, blue tongue

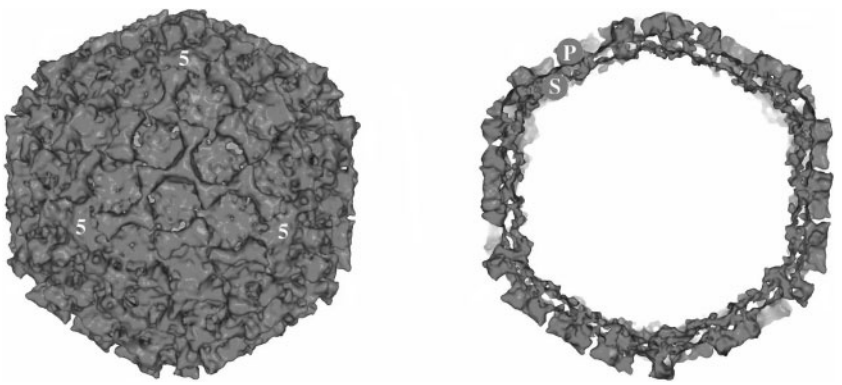

Fig. 4. Three-dimensional reconstruction of IBDV-VLP. The left panel shows the particle surface viewed down a position close to the threefold axis. Trimeric entities outline five- and sixfold depressions, defining a lattice that is characteristic of T = 13 icosahedral particles. In view of the shadowing data, the laevo configuration has been imposed. The right panels show a central slice through the reconstruction. A continuous shell (S) and a projecting domain (P) are visible.

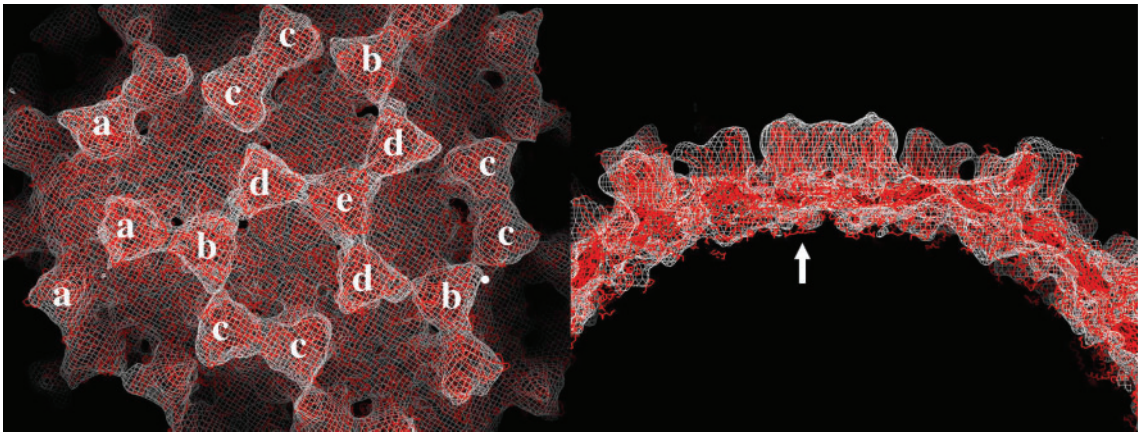

Fig. 5. Result of the fit of the atomic model of IBDV VP2 into the VLP reconstruction. The reconstruction electron density is represented together with the main chain of the VP2 atomic model. The VP2 molecule fits well into the electron density present in the reconstruction. The four independent trimers (a–d) and the one on the threefold axis (e), as defined by Bottcher *et al.* (1997), are labelled. The fivefold axes are surrounded by trimers a. On the left panel, the VP2 atomic models fitted in the reconstruction are seen from the top of the particle. On the right part, a central section of the reconstruction is shown with the fitted VP2 atomic models. The last 15 aa of VP2 that do not seem to be ordered in the absence of genomic RNA are indicated by an arrow.

virus VP7 and reovirus μ1 proteins) led to the same proposal (Coulibaly *et al.*, 2005).

The IBDV virion and VLP show, as expected, the same T = 13 laevo surface lattice. Because the VLP does not contain any genomic RNA, they have an enhanced tendency to flatten upon adsorption to the grid in comparison to the virion, and display poorer structural preservation. Similarly, freeze-drying structurally preserves viruses differently depending upon their fragility. IBDV particles that appear less fragile than IPNV with respect to their relative resistance to centrifugation conditions are better preserved during freeze-drying. The success in the determination of the hand of the surface lattice of icosahedral viruses thus highly depends upon their structural preservation upon freeze-drying and varies from one virus species to the next. Freeze-dried and shadowed birnavirus particles and VLPs are characterized by five- and sixfold holes that are easily differentiated. As expected from geometric considerations, five- and sixfold depressions have different sizes. Rotaviruses show similar characteristics (Roseto *et al.*, 1979). In addition, the VP2 trimers surrounding the fivefold axes have a stronger contrast than their sixfold axis homologues. This reflects different geometries that may account for particular function of VP2 such as the extrusion of newly transcribed mRNA from the virus capsid.

The reconstruction of IBDV-VLP embedded in vitrified ice shows a capsid composed by a thin continuous shell (S) and a protruding elongated projection (P). The reconstruction is similar to the reconstruction of the virion (Bottcher *et al.*, 1997; Caston *et al.*, 2001). The atomic model of VP2 can be fitted into the VLP reconstruction and occupies all the electron density that can be assigned to protein. The fusion protein VP3–GFP that is necessary for the efficient VLP formation (Chevalier *et al.*, 2002), and present in larger amounts than VP2 in the VLP, is not seen in the VLP electron density map. The four peptides derived from pVP2 processing and associated with VLP (Da Costa *et al.*, 2002) are also not detected. The GFP-fused VP3 in the VLP and VP3 in the virion are disordered in icosahedral symmetry. The fact that VP2 and VP3 have a different arrangement demonstrates that they have weak affinity. This observation is in agreement with the yeast two-hybrid experimental data showing that VP2 and VP3 do not interact significantly (Tacken *et al.*, 2000, 2003). With the observation that the presence of VP3 is crucial to the formation of a VLP (Chevalier *et al.*, 2002), it can be assumed that the affinity between VP3 and VP2 is increased by the formation of multimeric entities for both VP2 and VP3. VP1 and VP3 have been shown to interact (Tacken *et al.*, 2002) and to promote VLP assembly when the polyprotein and the polymerase VP1 are co-expressed (Chevalier *et al.*, 2004; Maraver *et al.*, 2003). It can thus be speculated that the viral polymerase will not be detected in the three-dimensional reconstruction of VLP containing VP1.

IBDV virions and the VLPs have similar icosahedral structure. Thus, the virus capsid does not appear to be dependent upon the presence of RNA. However, the genomic RNA appears to order the last 15 residues of VP2 in the virions. It has been shown that the packaging of the dsRNA segments in the bacteriophage phi6, a dsRNA virus of the family *Cystoviridae*, is sequential and postulated that it is associated with large capsid rearrangements (Bottcher *et al.*, 1997; Butcher *et al.*, 1997). In the case of birnaviruses, the

capsid protein VP2 having a unique icosahedral structure is not likely to participate in the RNA packaging mechanism. The interactions of VP3 with both VP1 and RNA, as well as a low symmetry arrangement increasing the interaction with the linear RNA segments, suggest that the complex VP1–VP3 might play an important role in the genome encapsidation.

ACKNOWLEDGEMENTS

We thank Lucienne Letellier (CNRS) and François-Xavier Le Gros (Mérial, Lyon, France) for their kind gift of T4 bacteriophage and IBDV suspensions, respectively, and Félix Rey for comments on the manuscript. We also thank Irina Gutsche and Armelle Vigouroux for carrying out chromatographies. This study was supported by the CNRS program 'Dynamique et réactivité des assemblages biologiques' and an ACI 'Microbiologie' from the French Research Ministry. J. P. acknowledges EMBO (ALTF 230/2002) and the European (HPMF-CTF-2002-01805) for supporting fellowships. C. C. was funded by a French MRT fellowship.

REFERENCES

Bayer, M. E. & Remsen, C. C. (1970). Bacteriophage T2 as seen with freeze-etching technique. *Virology* **40**, 703–718.

Birghan, C., Mundt, E. & Gorbalenya, A. E. (2000). A non-canonical Lon proteinase lacking the ATPase domain employs the ser-lys catalytic dyad to exercise broad control over the life cycle of a double-stranded RNA virus. *EMBO J* **19**, 114–123.

Bottcher, B., Kiselev, N. A., Stel'Mashchuk, V. Y., Perevozchikova, N. A., Borisov, A. V. & Crowther, R. A. (1997). Three-dimensional structure of infectious bursal disease virus determined by electron cryomicroscopy. *J Virol* **71**, 325–330.

Bradford, M. M. (1976). A rapid and sensitive method for the quantitation of microgram quantities of protein utilizing the principle of protein-dye binding. *Anal Biochem* **72**, 248–254.

Butcher, S. J., Dokland, T., Ojala, P. M., Bamford, D. H. & Fuller, S. D. (1997). Intermediates in the assembly pathway of the double-stranded RNA virus phi6. *EMBO J* **16**, 4477–4487.

Caston, J. R., Trus, B. L., Booy, F. P., Wickner, R. B., Wall, J. S. & Steven, A. C. (1997). Structure of L-A virus: a specialized compartment for the transcription and replication of double-stranded RNA. *J Cell Biol* **138**, 975–985.

Caston, J. R., Martinez-Torrecuadrada, J. L., Maraver, A., Lombardo, E., Rodriguez, J. F., Casal, J. I. & Carrascosa, J. L. (2001). C terminus of infectious bursal disease virus major capsid protein VP2 is involved in definition of the T number for capsid assembly. *J Virol* **75**, 10815–10828.

Chevalier, C., Lepault, J., Erk, I., Da Costa, B. & Delmas, B. (2002). The maturation process of pVP2 requires assembly of infectious bursal disease virus capsids. *J Virol* **76**, 2384–2392.

Chevalier, C., Lepault, J., Da Costa, B. & Delmas, B. (2004). The last C-terminal residue of VP3, glutamic acid 257, controls capsid assembly of infectious bursal disease virus. *J Virol* **78**, 3296–3303.

Conway, J. F. & Steven, A. C. (1999). Methods for reconstructing density maps of ''single'' particles from cryoelectron micrographs to subnanometer resolution. *J Struct Biol* **128**, 106–118.

Coulibaly, F., Chevalier, C., Gutsche, I., Pous, J., Navaza, J., Bressanelli, S., Delmas, B. & Rey, F. A. (2005). The birnavirus crystal structure reveals structural relationship among icosahedral viruses. *Cell* **120**, 761–772.

Da Costa, B., Chevalier, C., Henry, C., Huet, J. C., Petit, S., Lepault, J., Boot, H. & Delmas, B. (2002). The capsid of infectious bursal disease virus contains several small peptides arising from the maturation process of pVP2. *J Virol* **76**, 2393–2402.

Dobos, P., Hill, B. J., Hallett, R., Kells, D. T., Becht, H. & Teninges, D. (1979). Biophysical and biochemical characterization of five animal viruses with bisegmented double-stranded RNA genomes. *J Virol* **32**, 593–605.

Dubochet, J., Adrian, M., Chang, J. J., Homo, J. C., Lepault, J., McDowall, A. W. & Schultz, P. (1988). Cryo-electron microscopy of vitrified specimens. *Q Rev Biophys* **21**, 129–228.

Erickson, H. A. & Klug, A. (1971). Measurement and compensation of defocussing and aberrations by Fourier processing of electron micrographs. *Philos Trans R Soc Lond B Biol Sci* **261**, 105–118.

Escaig, J. & Nicolas, G. (1976). Cryofractures of biological material performed at very low temperatures in ultravacuum. *C R Acad Sci Hebd Seances Acad Sci D* **283**, 1245–1248.

Fernandez-Arias, A., Risco, C., Martinez, S., Albar, J. P. & Rodriguez, J. F. (1998). Expression of ORF A1 of infectious bursal disease virus results in the formation of virus-like particles. *J Gen Virol* **79**, 1047–1054.

Galloux, M., Chevalier, C., Henry, C., Huet, J. C., Costa, B. D. & Delmas, B. (2004). Peptides resulting from the pVP2 C-terminal processing are present in infectious pancreatic necrosis virus particles. *J Gen Virol* **85**, 2231–2236.

Grimes, J. M., Burroughs, J. N., Gouet, P., Diprose, J. M., Malby, R., Zientara, S., Mertens, P. P. & Stuart, D. I. (1998). The atomic structure of the bluetongue virus core. *Nature* **395**, 470–478.

Hill, C. L., Booth, T. F., Prasad, B. V., Grimes, J. M., Mertens, P. P., Sutton, G. C. & Stuart, D. I. (1999). The structure of a cypovirus and the functional organization of dsRNA viruses. *Nat Struct Biol* **6**, 565–568.

Lepault, J., Weiss, H., Homo, J. C. & Leonard, K. (1981). Comparative electron microscopic studies of partially negatively stained, freeze-dried and freeze-fractured cytochrome reductase membrane crystals. *J Mol Biol* **149**, 275–284.

Lombardo, E., Maraver, A., Castón, J. R., Rivera, J., Fernandez-Arias, A., Serrano, A., Carrascosa, J. L. & Rodriguez, J. F. (1999). VP1, the putative RNA-dependent RNA polymerase of infectious bursal disease virus, forms complexes with the capsid protein VP3, leading to efficient encapsidation into virus-like particles. *J Virol* **73**, 6973–6983.

Lu, G., Zhou, Z. H., Baker, M. L., Jakana, J., Cai, D., Wei, X., Chen, S., Gu, X. & Chiu, W. (1998). Structure of double-shelled rice dwarf virus. *J Virol* **72**, 8541–8549.

Ludert, J. E., Gil, F., Liprandi, F. & Esparza, J. (1986). The structure of the rotavirus inner capsid studied by electron microscopy of chemically disrupted particles. *J Gen Virol* **67**, 1721–1725.

Maraver, A., Clemente, R., Rodriguez, J. F. & Lombardo, E. (2003). Identification and molecular characterization of the RNA polymerase-binding motif of infectious bursal disease virus inner capsid protein VP3. *J Virol* **77**, 2459–2468.

Metcalf, P., Cyrklaff, M. & Adrian, M. (1991). The three-dimensional structure of reovirus obtained by cryo-electron microscopy. *EMBO J* **10**, 3129–3136.

Muller, H. & Becht, H. (1982). Biosynthesis of virus-specific proteins in cells infected with infectious bursal disease virus and their significance as structural elements for infectious virus and incomplete particles. *J Virol* **44**, 384–392.

Muller, H., Islam, M. R. & Raue, R. (2003). Research on infectious bursal disease – the past, the present and the future. *Vet Microbiol* **97**, 153–165.

Nakagawa, A., Miyazaki, N., Taka, J. & 9 other authors (2003). The atomic structure of rice dwarf virus reveals the self-assembly mechanism of component proteins. *Structure* **11**, 1227–1238.

Navaza, J. (2003). On the three-dimensional reconstruction of icosahedral particles. *J Struct Biol* **144**, 13–23.

Navaza, J., Lepault, J., Rey, F. A., Alvarez-Rua, C. & Borge, J. (2002). On the fitting of model electron densities into EM reconstructions: a reciprocal-space formulation. *Acta Crystallogr D Biol Crystallogr* **58**, 1820–1825.

Ona, A., Luque, D., Abaitua, F., Maraver, A., Caston, J. R. & Rodriguez, J. F. (2004). The C-terminal domain of the pVP2 precursor is essential for the interaction between VP2 and VP3, the capsid polypeptides of infectious bursal disease virus. *Virology* **322**, 135–142.

Ozel, M. & Gelderblom, H. (1985). Capsid symmetry of viruses of the proposed birnavirus group. *Arch Virol* **84**, 149–161.

Prasad, B. V., Yamaguchi, S. & Roy, P. (1992). Three-dimensional structure of single-shelled bluetongue virus. *J Virol* **66**, 2135–2142.

Prasad, B. V., Rothnagel, R., Zeng, C. Q., Jakana, J., Lawton, J. A., Chiu, W. & Estes, M. K. (1996). Visualization of ordered genomic RNA and localization of transcriptional complexes in rotavirus. *Nature* **382**, 471–473.

Reinisch, K. M., Nibert, M. L. & Harrison, S. C. (2000). Structure of the reovirus core at 3·6 A resolution. *Nature* **404**, 960–967.

Rodriguez Saint-Jean, S., Borrego, J. J. & Perez-Prieto, S. I. (2003). Infectious pancreatic necrosis virus: biology, pathogenesis, and diagnostic methods. *Adv Virus Res* **62**, 113–165.

Roseto, A., Escaig, J., Delain, E., Cohen, J. & Scherrer, R. (1979). Structure of rotaviruses as studied by the freeze-drying technique. *Virology* **98**, 471–475.

Tacken, M. G., Rottier, P. J., Gielkens, A. L. & Peeters, B. P. (2000). Interactions *in vivo* between the proteins of infectious bursal disease virus: capsid protein VP3 interacts with the RNA-dependent RNA polymerase, VP1. *J Gen Virol* **81**, 209–218.

Tacken, M. G., Peeters, B. P., Thomas, A. A., Rottier, P. J. & Boot, H. J. (2002). Infectious bursal disease virus capsid protein VP3 interacts both with VP1, the RNA-dependent RNA polymerase, and with viral double-stranded RNA. *J Virol* **76**, 11301–11311.

Tacken, M. G., Van Den Beuken, P. A., Peeters, B. P., Thomas, A. A., Rottier, P. J. & Boot, H. J. (2003). Homotypic interactions of the infectious bursal disease virus proteins VP3, pVP2, VP4, and VP5: mapping of the interacting domains. *Virology* **312**, 306–319.

von Einem, U. I., Gorbalenya, A. E., Schirrmeier, H., Behrens, S. E., Letzel, T. & Mundt, E. (2004). VP1 of infectious bursal disease virus is an RNA-dependent RNA polymerase. *J Gen Virol* **85**, 2221–2229.

Wang, B. C. (1985). Resolution of phase ambiguity in macromolecular crystallography. *Methods Enzymol* **115**, 90–112.